J|A|C|S ARTICLES

Published on Web 06/25/2009

Oxidation Unzipping of Stable Nanographenes into Joint Spin-Rich Fragments

Xingfa Gao,[†] Lu Wang,[†] Yuhki Ohtsuka,[†] De-en Jiang,[‡] Yuliang Zhao,[#,⊥] Shigeru Nagase,[*,†] and Zhongfang Chen[*,§]

Department of Theoretical and Computational Molecular Science, Institute for Molecular Science, Myodaiji, Okazaki 444-8585, Japan, Chemical Sciences Division, Oak Ridge National Laboratory, MS6201, Oak Ridge, Tennessee 37931-6201, Key Laboratory for Biomedical Effects of Nanomaterials and Nanosafety, Institute of High Energy Physics, Chinese Academy of Sciences, Beijing 100191, People's Republic of China, National Center for Nanoscience and Technology of China, Beijing 100080, People's Republic of China, and Department of Chemistry, Institute of Functional Nanomaterials, University of Puerto Rico, San Juan, Puerto Rico 00931

Received October 23, 2008; E-mail: nagase@ims.ac.jp; zhongfangchen@gmail.com

Abstract: When an all-benzenoid nanographene is linearly unzipped into oxygen-joined fragments, the oxidized benzenoid rings (aromatic sextets) selectively adopt the low-spin ($\Delta S = 0$) or high-spin conformation ($\Delta S = 1$) to yield the thermally most stable isomer. The selection of the conformation depends simply on the position of the aromatic sextets: the inner ones prefer the high-spin conformation, whereas the peripheral ones prefer the low-spin conformation. Therefore, the resulting most stable isomer has a total spin whose value equals the number of inner aromatic sextets (n_i) along the oxidizing line. The nanographene fragments contained in this isomer have a ferromagnetic spin coupling. Due to the tautomerization between the high-spin and low-spin conformations, there also exist other possible isomers with higher energies and with spins at ground state ranging from 0 to ($n_i - 1$). The rich geometrically correlated spins and the adjustable energy gaps indicate great potential of the graphene oxides in spintronic devices.

1. Introduction

Conventional magnets are pure transition metals, metal oxides, or metal alloys, which are inflexible and heavy and can be made only under high temperatures. For decades, researchers have attempted to create soft, light, and less energy-intensive magnets as alternatives. Principally, magnetism based upon metal-free materials is possible if the materials possess unpaired electrons that are subject to parallel alignments (ferromagnetic alignments) in the three-dimensional networks.[1−3] Along this road, several families of materials have been developed on the basis of organic radicals such as nitroxides,[4,5] polyarylmethyls,[6,7] verdazyls,[1,8] thiazyls,[9] and phenalenyls,[10] which exhibit magnetic orderings at very low temperatures. However, molecule-based magnets at room temperature are extremely rare despite intense investigations.[11]

When sp^2-carbon atoms are arranged into two-dimensional fused hexagons, they form a new material, namely, graphene.[12] The exotic electronic properties and potential applications in nanotechnologies[13−19] make graphene and related materials the superstar in advanced materials research.[20−22] The newly prepared graphene sheets are nonmagnetic themselves, which

[†] Institute for Molecular Science.
[‡] Oak Ridge National Laboratory.
[#] Institute of High Energy Physics, Chinese Academy of Sciences.
[⊥] National Center for Nanoscience and Technology of China.
[§] University of Puerto Rico.

(1) Blundell, S. J.; Pratt, F. L. *J. Phys.: Condens. Matter* **2004**, *16*, R771−R828.
(2) *Magnetic Properties of Organic Materials*; Lahti, P. M., Ed.; Marcel Dekker Inc.: New York, 1999.
(3) *Molecular Magnetism: New Magnetic Materials*; Ito K., Kinoshita N., Eds.; Kodansha Scientific: Tokyo, 2000.
(4) Likhtenshtein G. I.; Yamauchi J.; Nakatsuji, S.; Smirnov A. I.; Tamura R. *Nitroxides: Applications in Chemistry, Biomedicine, and Materials Science*; Wiley-VCH Verlag GmbH & Co. KGaA: Weinheim, 2008.
(5) Rajca, A.; Vale, M.; Rajca, S. *J. Am. Chem. Soc.* **2008**, *130*, 9099.
(6) Rajca, S.; Rajca, A. *J. Solid State Chem.* **2001**, *159*, 460.
(7) Rajca, A. *Chem.—Eur. J.* **2002**, *8*, 4835.
(8) Allemand, P. M.; Srdanov, G.; Wudl, F. *J. Am. Chem. Soc.* **1990**, *112*, 9391.
(9) Rawson, J. M.; Palacio, F. *Struct. Bonding (Berlin)* **2001**, *100*, 93.
(10) Itkis, M. E.; Chi, X.; Cordes, A. W.; Haddon, R. C. *Science* **2002**, *296*, 1443.
(11) Jain, R.; Kabir, K.; Gilroy, J. B.; Mitchell, K. A. R.; Wong, K. C.; Hicks, R. G. *Nature* **2007**, *445*, 291.
(12) Novoselov, K. S.; Geim, A. K.; Morozov, S. V.; Jiang, D.; Zhang, Y.; Dubonos, S. V.; Grigorieva, I. V.; Firsov, A. A. *Science* **2004**, *306*, 666.
(13) Yazyev, O. V.; Katsnelson, M. I. *Phys. Rev. Lett.* **2008**, *100*, 047209.
(14) Son, Y. W.; Cohen, M. L.; Louie, S. G. *Nature* **2006**, *444*, 347.
(15) Fernández-Rossier, J.; Palacios, J. J.; Brey, L. *Phys. Rev. B* **2007**, *77*, 205441.
(16) Muñoz-Rojas, F.; Fernández-Rossier, J.; Brey, L.; Palacios, J. *J. Phys. Rev. B* **2008**, *77*, 045301.
(17) Kan, E. J.; Li, Z.; Yang, J.; Hou, J. G. *J. Am. Chem. Soc.* **2008**, *130*, 4224.
(18) Freitag, M. *Nat. Nanotechnol.* **2008**, *3*, 455.
(19) Martins, T. B.; Silva, A. J. R. D.; Miwa, R. H.; Fazzio, A. *Nano Lett.* **2008**, *8*, 2293–2298.
(20) Geim, A. K.; Novoselov, K. S. *Nat. Mater.* **2007**, *6*, 183.
(21) Rogers, J. A. *Nat. Nanotechnol.* **2008**, *3*, 254.
(22) Brumfiel, G. *Nature* **2009**, *458*, 390.

limits some of their applications such as in spintronics. However, theoretical investigations revealed several intriguing phenomena. When cutting properly, the unpaired electrons can align at the zigzag edges of graphene, thus making graphene ferromagnetic along the edge.[23−25] When graphene is shaped into triangular nanographenes (NGs), it exhibits a nonzero total spin, with the spin simply scaling with size.[26−30] Unpaired electrons can also arise from the chemical reactions and defects of graphene.[31−34] In harmony with these predictions are the inspiring observations of room-temperature ferromagnetism for graphene oxide[35] and proton-bombarded graphite.[36,37] These findings have proven that NG polyradicals are striking building blocks for functional magnetic nanostructures that hold great promise to work at room temperature.

However, an obstacle exists between the theoretical models and practical nanodevices. The perfect ferromagnetic alignment of unpaired electrons along the one-dimensional zigzag edge of graphene is unstable and can be maintained only within a short range at temperatures above absolute zero;[13,38] on the other hand, the thermally driven face-to-face stacking of two NG radicals is known to cause a strong antiferromagnetic coupling of the spins, which forces the unpaired electrons into antiparallel alignments and cancels the total magnetic moments.[39−41] Therefore, it is highly desired to design a thermally stable assembly of NG radicals with ferromagnetic spin couplings.

Top-down approaches to nanometer-sized graphenes have great technical implications for molecular electronics, and breaking down the stable π-system in graphene by oxidation is a commonly employed technique;[42−55] among them, oxidizing NGs provides a conceptually simple way to unzip the π-system.[43,48−50] The NGs obtained by organic synthesis,[56] also known as polycyclic aromatic hydrocarbons (PAHs), are stable nonmagnetic (closed-shell singlet) molecules of nanometer sizes, whose structures and properties have been well characterized, and thus provide practically feasible models for molecule and device design. In this article, we seek to understand and predict how the π-system of such NGs respond to linear oxidation that cuts them into oxygen-joined NG fragments.

Guided by experiments, we chose the all-benzenoid hydrocarbons **1**−**3**, which have been fully characterized,[56,57] as our oxidation targets. These three NGs satisfy Clar's aromatic sextet rule[58] with exclusive Clar's structure, in which all the π-electrons form separated benzenoid rings (aromatic sextets) (Figure 1) and thus have great stability.[58,59] Our computations demonstrated that the linear oxidation of **1**−**3** results in a large number of isomers of NG oxides with different geometries and spin values. Importantly, the isomers with high spins, i.e., those consisting of NG radicals with ferromagnetic spin coupling, have the largest thermal stabilities. Therefore, our studies open a new way for realization of NG-based molecular magnets.

2. Computational Details

All geometry optimizations and energy calculations were performed using the Gaussian 03 program.[60] Geometries were optimized using the B3LYP method[61−63] in combination with the 6-31G(d) basis set (B3LYP/6-31G(d)).[64,65] For all the singlet states, the spin-restricted (non-spin-polarized) scheme (RB3LYP) was used, and for all the triplets, quintets, and heptets, the spin-unrestricted (spin-polarized) scheme (UB3LYP) was employed. In each computation, the symmetry was constrained to C_1, C_s, or C_{2v} depending on the point group symmetry of the respective structures; no additional geometric constraints were used. Each NG oxide studied here has a large number of local minima on the potential energy surfaces; to locate them, one needs proper input of spin multiplicities and initial structures, especially the local structures

(23) Fujita, M.; Wakabayashi, K.; Nakada, K.; Kusakabe, K. *J. Phys. Soc. Jpn.* **1996**, *65*, 1920.
(24) Castro Neto, A. H.; Guinea, F.; Peres, N. M. R.; Novoselov, K. S.; Geim, A. K *Rev. Mod. Phys.* **2009**, *81*, 109, and references therein.
(25) Enoki, T.; Kobayashi, Y.; Fukui, K. I. *Int. Rev. Phys. Chem.* **2007**, *26*, 609.
(26) Ezawa, M. *Phys. Rev. B* **2007**, *76*, 245415.
(27) Ezawa, M. *Physica E* **2008**, *40*, 1421.
(28) Yazyev, O. V.; Wang, W. L.; Meng, S.; Kaxiras, E. *Nano Lett.* **2008**, *8*, 766.
(29) Wang, W. L.; Meng, S.; Kaxiras, E. *Nano Lett.* **2008**, *8*, 241.
(30) Fernández-Rossier, J.; Palacios, J. J. *Phys. Rev. Lett.* **2007**, *99*, 177204.
(31) Yazyev, O. V.; Helm, L. *Phys. Rev. B* **2007**, *75*, 125408.
(32) Kumazaki, H.; Hirashima, D. S. *J. Phys. Soc. Jpn.* **2007**, *76*, 064713.
(33) Palacios, J. J.; Fernández-Rossier, J.; Brey, L. *Phys. Rev. B* **2008**, *77*, 195428.
(34) Yazyev, O. V. *Phys. Rev. Lett.* **2008**, *101*, 037203.
(35) Wang, Y.; Huang, Y.; Song, Y.; Zhang, X.; Ma, Y.; Liang, J.; Chen, Y. *Nano Lett.* **2009**, *9*, 220.
(36) Han, K. H.; Spemann, D.; Esquinazi, P.; Höhne, R.; Riede, V.; Butz, T. *Adv. Mater.* **2003**, *15*, 1719.
(37) Esquinazi, P.; Spemann, D.; Höhne, R.; Setzer, A.; Han, K. H.; Butz, T. *Phys. Rev. Lett.* **2003**, *91*, 227201.
(38) Mermin, N. D.; Wagner, H. *Phys. Rev. Lett.* **1966**, *17*, 1133.
(39) Harigaya, K. *J. Phys.: Condens. Matter* **2001**, *13*, 1295–1302.
(40) Lee, H.; Son, Y. W.; Park, N.; Han, S.; Yu, J. *Phys. Rev. B* **2005**, *72*, 1774431.
(41) Takano, Y.; Taniguchi, T.; Isobe, H.; Kubo, T.; Morita, Y.; Yamamoto, K.; Nakasuji, K.; Takui, T.; Yamaguchi, K. *J. Am. Chem. Soc.* **2002**, *124*, 11122.
(42) Kudin, K. N.; Ozbas, B.; Schniepp, H. C.; Prud'homme, R. K.; Aksay, I. A.; Car, R. *Nano Lett.* **2008**, *8*, 36.
(43) Schniepp, H. C.; Li, J. L.; McAllister, M. J.; Sai, H.; Herrera-Alonso, M.; Adamson, D. H.; Prud'homme, R. K.; Car, R.; Saville, D. A.; Aksay, I. A. *J. Phys. Chem. B* **2006**, *110*, 8535.
(44) Ci, L.; Xu, Z.; Wang, L.; Gao, W.; Ding, F.; Kelly, K. F.; Yakobson, B. I.; Ajayan, P. M. *Nano Res.* **2008**, *1*, 116.
(45) Hod, O.; Barone, V.; Peralta, J. E.; Scuseria, G. E. *Nano Lett.* **2007**, *7*, 2295.
(46) Gómez-Navarro, C.; Weitz, R. T.; Bittner, A. M.; Scolari, M.; Mews, A.; Burghard, M.; Kern, K. *Nano Lett.* **2007**, *7*, 3499.
(47) Zhu, J. *Nat. Nanotechnol.* **2008**, *3*, 528.
(48) Yumura, T.; Kertesz, M. *Chem. Mater.* **2007**, *19*, 1028.
(49) Ajayan, P. M.; Yakobson, B. I. *Nature* **2006**, *441*, 818.
(50) (a) Li, J. L.; Kudin, K. N.; McAllister, M. J.; Prud'homme, R. K.; Aksay, I. A.; Car, R. *Phys. Rev. Lett.* **2006**, *96*, 176101. (b) Li, Z.; Zhang, W.; Luo, Y.; Yang, J.; Hou, J. G. *J. Am. Chem. Soc.* **2009**, *131*, 6320.
(51) Cai, W.; Piner, R. D.; Stadermann, F. J.; Park, S.; Shaibat, M. A.; Ishii, Y.; Yang, D.; Velamakanni, A.; An, S. J.; Stoller, M.; An, J.; Chen, D.; Ruoff, R. S. *Science* **2008**, *321*, 1815.
(52) Li, X.; Wang, X.; Zhang, L.; Lee, S.; Dai, H. *Science* **2008**, *319*, 1229.
(53) Gilje, S.; Han, S.; Wang, M.; Wang, K. L.; Kaner, R. B. *Nano Lett.* **2007**, *7*, 3394.
(54) Stankovich, S.; Dikin, D. A.; Dommett, G. H. B.; Kohlhaas, K. M.; Zimney, E. J.; Stach, E. A.; Piner, R. D.; Nguyen, S. T.; Ruoff, R. S. *Nature* **2006**, *442*, 282.
(55) Mkhoyan, K. A.; Contryman, A. W.; Silcox, J.; Stewart, D. A.; Eda, G.; Mattevi, C.; Miller, S.; Chhowalla, M. *Nano Lett.* **2009**, *9*, 1058.
(56) Müllen, K.; Rabe, J. P. *Acc. Chem. Res.* **2008**, *41*, 511, and references therein.
(57) Watson, M. D.; Fechtenkötter, A.; Müllen, K. *Chem. Rev.* **2001**, *101*, 1267, and references therein.
(58) Clar E. *The Aromatic Sextet*; Wiley-VCH: London, 1972.
(59) Moran, D.; Stahl, F.; Bettinger, H. F.; Schaefer, H. F., III; Schleyer, P. V. R. *J. Am. Chem. Soc.* **2003**, *125*, 6746.
(60) Frisch, M. J.; et al. *Gaussian 03*; Gaussian, Inc.: Wallingford, CT, 2004.
(61) Becke, A. D. *Phys. Rev. A* **1988**, *38*, 3098.
(62) Lee, C.; Yang, W.; Parr, R. G. *Phys. Rev. B* **1988**, *37*, 785.
(63) Becke, A. D. *J. Chem. Phys.* **1993**, *98*, 5648.
(64) Hehre, W. J.; Ditchfield, R.; Pople, J. A. *J. Chem. Phys.* **1972**, *56*, 2257.
(65) Hariharan, P. C.; Pople, J. A. *Mol. Phys.* **1974**, *27*, 209.

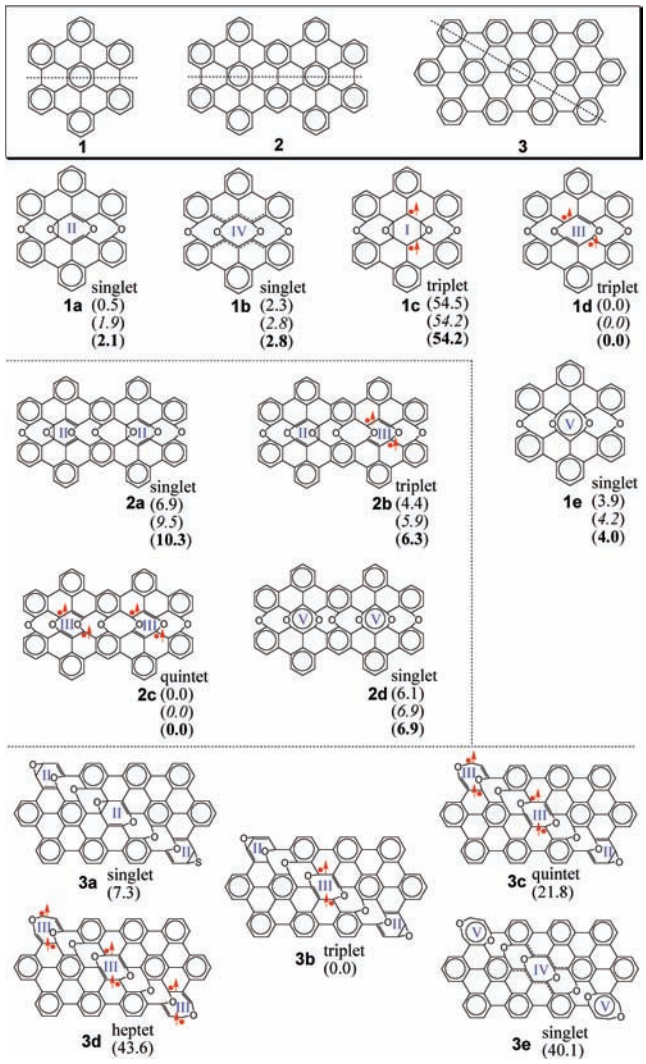

Figure 1. All-benzenoid polycyclic aromatic hydrocarbons (**1**−**3**) and the oxides. Spin multiplicities are given; relative energies (E_{rel}, regular print), ZPE-corrected E_{rel} (italic print) and relative Gibb's free energies at 298.15 K (G_{rel}, bold print) at the (U)B3LYP/6-31G(d) level of theory are given in parentheses. The unit for energies is kcal/mol; I−V label the conformations of the oxidized aromatic benzenoid ring (see text). The dashed lines (oxidizing lines) of **1**−**3** show the directions along which they are oxidized. The bond orders labeled for each structure are intended to give a straightforward understanding of the electronic configuration, which do not necessarily indicate the bond lengths.

along the oxidizing lines, to start the geometry optimizations. Therefore, the NG oxide structures reported in this work were located by trial and error. For **1a**−**e** and **2a**−**d**, frequency analyses were performed at the same level of theory on the basis of the optimized geometries to confirm that the optimized structures are true local minima and calculate the zero-point energies (ZPEs) and entropies. Because the spin-restricted single-determinant wave functions for NG structures might have the RHF → UHF instability, the stabilities of the wave functions of **1a**, **1b**, and **1e** were checked using the "stable" keyword; no such instability was found. In the geometry optimization and energy calculation of **4a**, **4b**, or **4c**, one-dimensional (1-D) periodical boundary conditions (PBC) were applied along the oxidizing line, with 10 *k*-points for the sampling of the Brillouin zone. In the Gaussian 03 input file, this was realized by defining one transition vector (Tv) along the oxidizing line of the unit cell, in the molecule specification part, and by using the option "PBC(NKPoint=10)" in the route section. The molecular orbitals (MOs) of **1d** and **6** were calculated using the spin-restricted open-shell B3LYP (ROB3LYP) method in conjunction with the 6-31G(d) basis set (ROB3LYP/6-31G(d)), on the basis of the geometries optimized at the same level of theory.

To confirm the performance of the 6-31G(d) basis set, we calculated the relative stability for **2a**−**c** with a larger basis set, 6-311G(d)[66,67] (B3LYP/6-311G(d)), which gave the same relative stabilities as B3LYP/6-31G(d) does (see Table S1 of the Supporting Information, SI). Therefore, all energies discussed in this article were obtained with the (U)B3LYP/6-31G(d) method. At the level of (U)B3LYP/6-31G(d), the calculated expectation values of the S^2 operator ($\langle S^2 \rangle$) are 0.0, 2.1, 6.2, and 12.3 for the closed-shell singlet, triplet, quintet, and heptet, respectively, which correspond to the total spins of 0, 1, 2, and 3 with only small spin combinations (<5%) (Table S2 of the SI).

The effective exchange integral (J_{eff}) for the intramolecular NG interaction of **1d** was calculated with the equation proposed by Yamaguchi et al.[41]

$$J_{eff} = ({}^{LS}E - {}^{HS}E)/({}^{HS}\langle S^2 \rangle - {}^{LS}\langle S^2 \rangle)$$

where ${}^{LS}E$ and ${}^{HS}E$ denote the total energies of the broken-symmetry singlet and triplet states of **1d**, and ${}^{LS}\langle S^2 \rangle$ and ${}^{HS}\langle S^2 \rangle$ denote the respective total angular momentums. ${}^{LS}E$ was obtained through single-point (SP) energy calculation at the UB3LYP/6-31G(d) level, on the basis of the geometry of **1d** (triplet) optimized at the same level of theory; in the SP calculation, the "guess=mix" option was used to generate a broken-symmetry initial guess for the spin-singlet configuration.

3. Results and Discussion

3.1. Geometries and Spins of NG Oxides with the Highest Relative Stability. We first studied the linear oxidation of **1** along the dashed line as shown in Figure 1. This oxidizes one benzenoid ring and two single bonds according to Clar's structure of **1** and leads to tetroxide. Geometry optimizations at the (U)B3LYP/6-31G(d) level of theory led to five energy minima for the tetroxide, **1a**−**e**, which have different spins or geometries (Figure 1). The lowest-energy isomer, **1d**, is triplet (total spin $S_{tot} = 1$), and its energy is lower than the lowest-energy singlet ($S_{tot} = 0$), **1a**, by 1.9 kcal/mol. The wave functions of singlets **1a**, **1b**, and **1e** are stable, suggesting that a stable open-shell singlet state does not exist, unlike rectangular-shaped NGs.[68−71] The linear oxidation of **2** along the dashed line oxidizes two benzenoid rings and three single bonds (Figure 1), for which our computations revealed more energy minima (see Figure 1 and Figure S1 of the SI). Again, the isomer with the highest spin, **2c**, has the lowest energy.

The linear oxidation of **3** along the dashed line oxidizes three benzenoid rings (Figure 1). Unlike **1** or **2**, where the oxidized benzenoid rings are all located in the inner area of the molecular plane, two out of the three oxidized benzenoid rings in **3** are at the peripheral edge. Unlike **1** or **2**, the triplet **3b** is the lowest-energy isomer, rather than the higher-spin heptet **3d** ($S_{tot} = 3$, the highest in this case) or quintet **3c** (Figure 1).

We further examined linear oxidation of infinite-size graphene nanoribbons **4**, which being infinite have only inner benzenoid rings, along the dashed line (see Figure 2). Figure 2 shows the optimized geometries and magnetic moments for the unit cells

(66) Krishnan, R.; Binkley, J. S.; Seeger, R.; Pople, J. A. *J. Chem. Phys.* **1980**, *72*, 650.
(67) McLean, A. D.; Chandler, G. S. *J. Chem. Phys.* **1980**, *72*, 5639.
(68) Hod, O.; Peralta, J. E.; Scuseria, G. E. *Phys. Rev. B* **2007**, *76*, 233401.
(69) Hod, O.; Barone, V.; Scuseria, G. E. *Phys. Rev. B* **2008**, *77*, 035411.
(70) Jiang, D. E.; Sumpter, B. G.; Dai, S. *J. Chem. Phys.* **2007**, *127*, 124703.
(71) Gao, X.; Zhou, Z.; Zhao, Y.; Nagase, S.; Zhang, S. B.; Chen, Z. *J. Phys. Chem. C* **2008**, *112*, 12677.

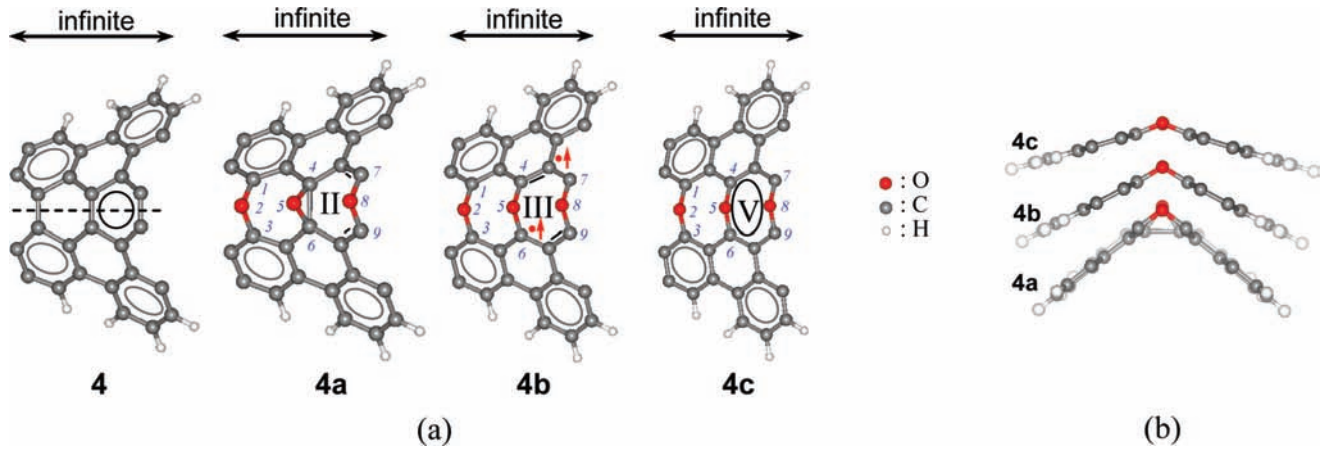

Figure 2. Unit cells **4** and **4a**−**c** of one-dimensional infinite graphene oxide optimized at the B3LYP/6-31G(d) level of theory with 10 k-points for the samplings of Brillouin zones. (a) Top view and (b) side view. II, III, and V label the conformations of the oxidized aromatic benzenoid rings; the dashed line (oxidizing line) of **4** shows the direction of oxidation.

Table 1. Calculated Magnetic Moments (M), Relative Energies (E_{rel}), and Geometric Parameters for Unit Cells **4a**−**c**[a]

		4a	4b	4c
M (μ_B)		0.0	2.0	0.0
E_{rel} (kcal/mol)		6.2	0.0	2.1
bond length (Å) of C−O	*1*−*2*	1.384	1.380	1.364
	4−*5*	1.413	1.379	1.346
	7−*8*	1.386	1.379	1.346
bond angle (deg) of C−O−C	*1*−*2*−*3*	106.4	118.7	133.7
	4−*5*−*6*	71.2	118.8	138.5
	7−*8*−*9*	106.0	118.8	138.5

[a] Calculated C−O bond length and C−O−C bond angle for **5** (Figure 4c) are 1.331 Å and 134.4°, respectively.

Table 2. Five Conformations of Oxidized Benzenoid Ring

no.	structure[a]	hybrid state of oxygen	contribution of net spin electrons (net spin, ΔS)
I	epoxide/epoxide	sp^3	2 (1)
II	epoxide/ether	sp^3	0 (0)
III	ether/ether	sp^3	2 (1)
IV	epoxide/epoxide	sp^3	0 (0)
V	(10e)-aromatic ring	sp^2	0 (0)

[a] See Figure 1 for the structures of I−V.

of one-dimensional infinite graphene oxides, while Table 1 shows their relative stabilities. The selection of III for the oxidized benzenoid ring indeed gives **4b** the largest thermal stability, which is energetically lower than **4a** (selection of II) and **4c** (selection of V) by 6.2 and 2.1 kcal/mol, respectively (Table 1).

To understand why oxidation products of **1**, **2**, **3**, and **4** adopt their respective lowest-energy spins, here we analyze the various scenarios of linear oxidation of a benzenoid ring. In the optimized geometries of **1a**−**e**, **2a**−**d**, **3a**−**e**, and **4a**−**c**, oxygen atoms attached on the pristine single bonds of **1**, **2**, **3**, and **4** always adopt the open-bonded ether-like bridge structure, not contributing any net spin ($\Delta S = 0$), whereas those attached on the benzenoid rings can adopt five types of confirmation with different geometries or spins, which are labeled with "I"−"V" in Figure 1 and Table 2. The high-spin conformation III ($\Delta S = 1$) is energetically the most preferred pattern if the oxidized benzenoid ring is localized in the inner area of NG; however, the low-spin conformation II ($\Delta S = 0$) is energetically the most favorable if it is located at the peripheral edges. This different preference is because the unpaired electrons generated in the inner area can receive stabilization from the conjugation, whereas those at the edge cannot. This stabilization also explains why **1d**, **2c**, **3b**, and **4b** are the lowest-energy oxides for the linear oxidations of **1**, **2**, **3** and **4**, respectively (Figure 1).

3.2. Structural Tautomerization and Spin Conversion of NG Oxides. Inspecting the energetic relation between the respective lowest-energy isomers and the other isomers, we observed that the high-spin conformation III of the oxidized benzenoid ring can tautomerize to the zero-spin conformation II with an energy penalty of 1.9−7.3 kcal/mol and with the following relationship of spin conversion,

$$S_{III} = S_{II} + 1 \quad (1)$$

where S_{III} and S_{II} denote the total spins for the isomers with the oxidized benzenoid ring of III and II types, respectively. The structural tautomerization and spin conversion between **2a**, **3a**, and **4a** are illustrated in Figure 3. The geometry/spin relationship indeed follows eq 1. The largest spin density is localized on III, whereas no spin density is on II; this distribution is well consistent with the above analysis that conformations II and III contribute net spins of 0 and 2, respectively (Table 2). Similarly, the tautomerization between conformations II and III explains the existence of **1a**, **3a**, **3c**, **3d**, and **4a**, and the tautomerization from III to IV or V accounts for the existence of other isomers such as **1b**, **1e**, **2d**, **3e**, and **4c**.

In addition to altering spin states, the structural tautomerization exerts a strong influence on the molecular shape, especially the joint angle between the two NG fragments. The influence of joint angle is illustrated in Figure 2c, by layering **4a**, **4b**, and **4c**. These three compounds have joint angles of about 98°, 119°, and 136°, respectively, because of the respective C−O−C bond angles they contain (Table 1). The involvement of an epoxide unit in **4a** accounts for its relatively small joint angle, and the joint angle of **4b** is also reasonably comparable to the C−O−C bond angle of ethers, which is around 110°. To study the reason for the significantly large joint angle of **4c**, we list the C−O bond lengths and C−O−C bond angles of the three compounds in Table 1. Accompanying the larger C−O−C bond angles of **4c** are the shortening of C−O bond lengths and the larger planarity ring of V. The orbital hybridization theory[72] is very useful in explaining the shapes of molecules. On the basis

(72) Pauling, L. *J. Am. Chem. Soc.* **1931**, *53*, 1367.

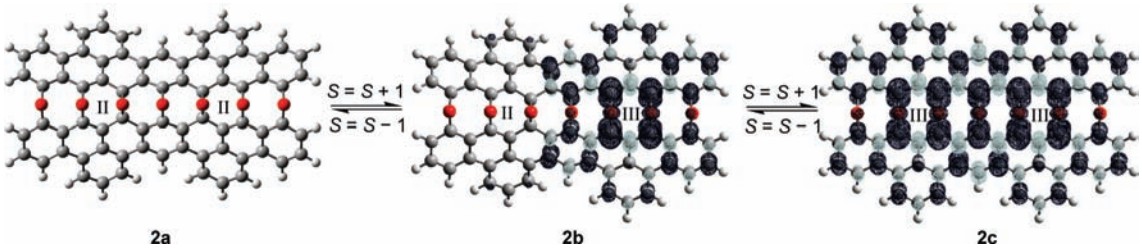

Figure 3. Spin conversion and spin density distribution of **2a**, **2b**, and **2c**. Dark color, majority spin; light color, minority spin; the setting of atom colors is the same as in Figure 2.

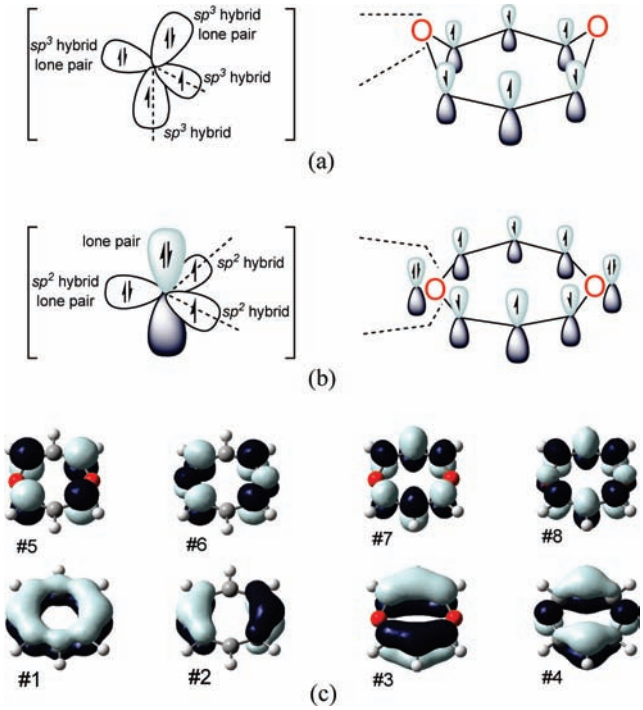

Figure 4. Delocalized atomic orbitals of oxidized benzenoid ring (a) III and (b) V. (c) Delocalized MOs of prototype molecular **5** ($C_6O_2H_6$) that resembles structure V. The insets of (a) and (b) show the orbital hybridization of the respective oxygen atoms. MOs #1−5 of (c) are doubly occupied by a total of 10 electrons, while MOs #6−8 of (c) are vacant orbitals.

of these geometric characters, we propose that unlike oxidized benzenoid rings II and III where oxygens are sp^3-hydridized (for III, see Figure 4a), both oxygens in V partially adopt sp^2-hydrid state, with one of the lone pairs of electrons delocalized into the ring (see Figure 4b). Because structure V has 10 π-electrons, it obeys the $4n+2$ rule and is aromatic. For verification, we calculated the molecular orbitals (MOs) for $C_6O_2H_6$ (denoted as **5**), the prototype molecule of structure V. The result shows that **5** is indeed planar, has a closed-shell singlet ground state, and has eight delocalized MOs (see Figure 4c) derived from the eight atomic orbitals, as shown in Figure 4b. Due to the formation of the C−O aromatic bond, the C−O bond length of **5** is shortened to 1.331 Å. Therefore, the types of hybridization we proposed for the oxygens in the NG oxides profoundly rationalize the geometry and spin of ring V, as well as the joint angle of **4c**. Because of the difference in geometric demand, the coexistence of V with III is sterically more hindered. Therefore, the isomerization of III to V does not deserve further attention; neither does the isomerization to I or IV, because I causes a much larger penalty of energy and IV has a similar geometry/spin to II but also causes a larger penalty of energy. Because the energy barriers for all tautomerizations are not considered in this study, care should be taken when using the above results to make conclusions regarding the kinetic feasibility of the process.

3.3. Magnetic Interaction between NG Fragments of Individual NG Oxides. Because the NG oxides with high-spin ground states, e.g., **1d** and **2c**, can be viewed as two NG fragments bridged with oxygen atoms, one wonders (1) the correlation between the electronic structures of the NG oxides with their fragments and (2) the magnetic interaction between both fragments in the individual NG oxides.

Taking **1d** as an example, it can be deemed as two triangular units **6** connected with four oxygen atoms along the zigzag edges, where the oxygens simultaneously replace the terminating hydrogens of the edges. **6** is a triangular-shaped NG with an odd number of carbon atoms, whose electronic structures have been reported recently.[26−30] Our calculation suggests that **6** has a doublet ground state, which is consistent with the recent results.[26−30] To compare the electronic structure of **6** and **1d**, we show the shapes and energies of the singly occupied molecular orbitals (SOMO) and the two neighboring MOs of **6** in Figure 5a and those of the two SOMOs and the neighboring MOs of **1d** in Figure 5b. According to Figure 5, the two SOMOs of **1d** can be characterized as the combination of the SOMO of **6**; however, both SOMOs of **1d** have the same energies as that of **6**. Similarly, the next-HOMO − 1 and next-HOMO − 2 of **1d** are the combination of the next-HOMO of **6**, and the next-LUMO and next-LUMO + 1 of **1d** are the combination of the next LUMO of **6**; again, the corresponding orbital energies of **1d** are nearly the same as those of the corresponding primitive ones of **6**. These results indicate that the orbital interactions between the two fragments are very weak and that **1d** keeps the main electronic features of the fragments.

The effective exchange integral (J_{eff}) calculated for **1d** is 197.5 cm^{-1}, which implies that the two magnetic centers, i.e., the two NG fragments of **1d**, have a ferromagnetic spin coupling;[41] in other words, in **1d**, the spins prefer a parallel alignment. Such a preference agrees with Figure 6, which shows the SOMOs of **1d** in the broken-symmetry low-spin state: the α and β SOMOs, i.e., the magnetic orbitals, are distributed separately on the two fragments, out of phase from each other, and hardly yield orbital overlap. The ferromagnetic coupling of segregated magnetic moments in **1d** is in sharp contrast to many other examples of graphene nanostructures, where the localized magnetic moments tend to couple antiferromagnetically.[39−41,73]

3.4. Linear Oxidation of NGs and NG Derivatives with Arbitrary Shapes. To further rationalize the selection and conversion of geometry/spin and predict the spin ground state for linearly oxidized all-benzenoid NGs with arbitrary shapes,

(73) Wang, W. L.; Yazyev, O. V.; Meng, S.; Kaxiras, E. *Phys. Rev. Lett.* **2009**, *102*, 157201.

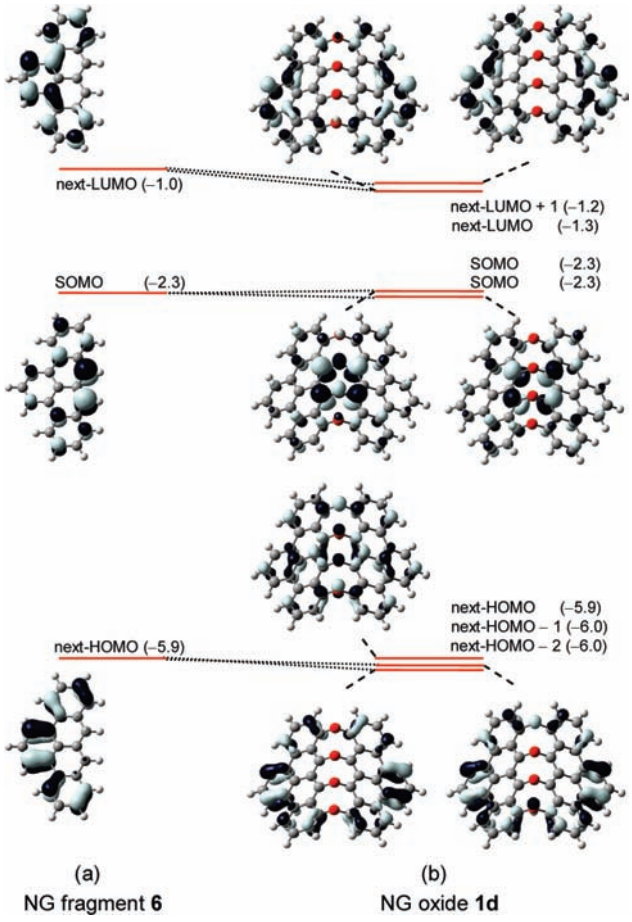

Figure 5. Some MOs of (a) NG fragment **6** and (b) NG oxide **1d** at the ground states calculated at the ROB3LYP/6-31G(d)//ROB3LYP/6-31G(d) level of theory. Orbital energies (in eV) are given in parentheses.

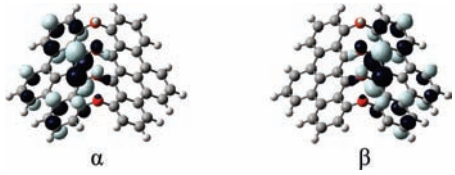

Figure 6. α and β SOMOs of **1d** in the broken-symmetry low-spin states at the UB3LYP/6-31G(d)//UB3LYP/6-31G(d) level of theory.

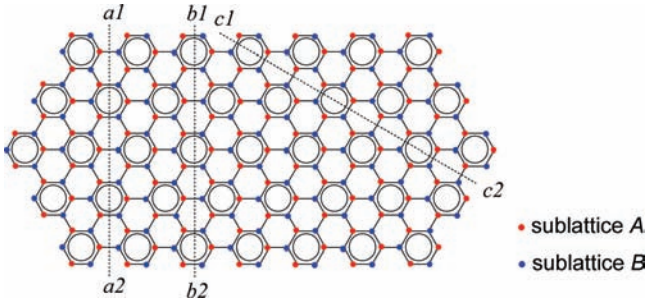

Figure 7. Split of stable NG along *a1*−*a2*, *b1*−*b2*, and *c1*−*c2*.

we considered the crystal structure of graphene, i.e., carbon atoms arranged in a hexagonal structure consisting of a triangular lattice with a base of two atoms per unit cell, sublattices *A* and *B* (Figure 7). Previous works have found a simple equation to determine the total spin of the ground state of this kind of material, $S = |N_A - N_B|/2$, where N_A and N_B are the numbers of atoms belonging to the two sublattices. This equation, known as Lieb's theorem, was first proved by Lieb in 1989, on the basis of an approximate model, the half-filled Hubbard model on some bipartite lattices,[74] and recently confirmed by first-principle calculations.[28−30] According to these results, the carbon atoms belonging to the different sublattices have different spin orientations (up or down), whose balance determines the net spin of NG. Here, with the aid of Lieb's theorem, we extend the geometry and spin selection rule we have found above to predict the geometries/spins for the linearly oxidized all-benzenoid NGs with arbitrary shapes.

Because of the balanced population of sublattices *A* and *B*, any all-benzenoid hydrocarbon has zero total spin (Figure 7) according to Lieb's theorem.[74] This balance is clearly due to the balance of *A* and *B* in each elemental benzenoid ring ($N_A = N_B = 3$). However, when split into two separated fragments or fragments joined by σ-bonds along a straight line, sublattice imbalance arises: the split of every one ring leads to the generation of two unbalanced sites, i.e., *A* and *B*, with a ferromagnetic interaction and, thus, increases the total spin by 1. One may therefore write the total spin of the two fragments as $S_{tot} = n$, where *n* is the number of split benzenoid rings. In the case of linear oxidation, such split corresponds to the formation of III-type oxygen bridges for the oxidized benzenoid ring, and thus *n* is the number of rings that are oxidized to III. The formation of II does not change the spin because the epoxidation converts the unpaired *A* and *B* into an sp^3 hybrid state and thus removes both from the π-conjugated system. The formation of V also does not change the spin because *A* and *B* are again paired in the (10e)-aromatic ring therein. Since peripheral rings prefer to form II-type and the inner rings prefer to form III-type oxygen bridges, one may predict that a linear oxidation gives rise to oxides with

$$S_g = n_i \qquad (2)$$

where S_g is the total spin at ground state and n_i is the number of inner rings along the oxidation line. Therefore, eq 2 nicely predicts the spin ground state for linearly oxidized all-benzenoid NGs with arbitrary shapes; in combination with eq 1, other low-lying states can also be predicted. For example, in Figure 7, linear oxidations along *a1*−*a2*, *b1*−*b2*, and *c1*−*c2* will lead to ground-state oxides with $S_g = 2$, 1, and 2, respectively (according to eq 2), and these oxides will isomerize to give at least $(n_i - 1)$ higher-energy isomers with $S = 0$ through $(n_i - 1)$, respectively (according to eq 1).

Equations 1 and 2 are also applicable for NG derivatives. For example, reducing or expanding the π-conjugation of **2** to $\mathbf{2}H_4$ or $\mathbf{2}C_4$ does not change the sublattice balance as in **2**; consequently, the ground states of the heptoxide of both remain quintet, the same as **2**, only adjusting energy levels (see Figure 8). Edge oxidation is likely to occur in the reactions of NG. Because edge oxidation does not change the sublattice balance, similar to the case of $\mathbf{2}H_4$, eqs 1 and 2 are applicable. So, the energy gaps of the oxide can be engineered via chemical reactions without destroying the main spin property.

4. Conclusion

In summary, we have shown that when an all-benzenoid NG is linearly unzipped into oxygen-joined fragments, the geom-

(74) Lieb, E. H *Phys. Rev. Lett.* **1989**, *62*, 1201. Erratum. *Phys. Rev. Lett.* **1989**, *62*, 1927.

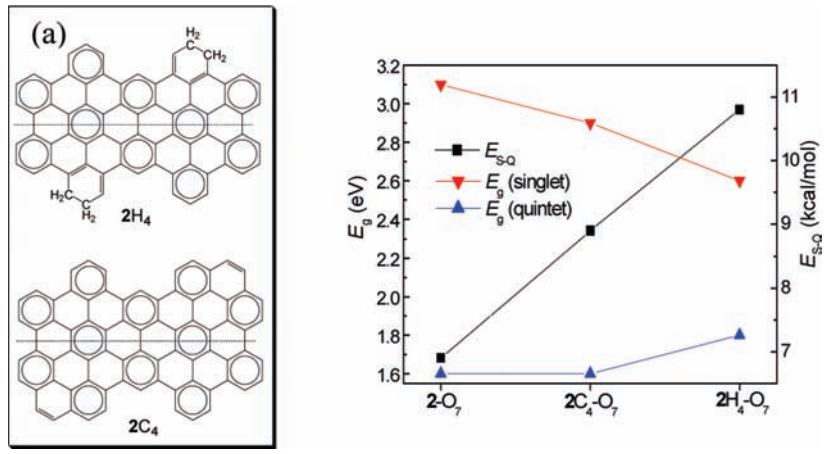

Figure 8. Energy levels of heptoxides of **2**, **2**H_4, and **2**C_4 at the (U)B3LYP/6-31G(d) level of theory; these oxides are generated through the linear oxidations along the respective dashed lines. (a) Derivatives of **2**. (b) E_g(singlet), HOMO−LUMO gap of the lowest-energy singlet state; E_g(quintet), (α-HOMO)−(β-LUMO) gap of the lowest-energy quintet; $E_{S\text{-}Q}$, the singlet−quintet split energy, E(singlet) − E(quintet). Lines are guides to the eye.

etries and spins of the resulting oxides in the ground state can be predicted. To yield the most stable isomer, the oxidized benzenoid ring (aromatic sextet) favorably adopts the low-spin conformation II ($\Delta S = 0$) if it is located at the periphery of NG, whereas it adopts high-spin conformation III ($\Delta S = 1$) if it is in the inner plane. Consequently, the total spin of the oxide in the ground state equals the number of inner aromatic sextets (n_i) along the oxidizing line. Due to the tautomerization between the high-spin and low-spin conformations, there exist a rich number of other possible isomers with higher relative energies and spins ranging from 0 to ($n_i - 1$). The rich geometrically correlated spins, adjustable energy gaps, and high thermal stabilities of NG oxides open new opportunities for us to realize the NG-based molecular magnets. We believe that further experimental and theoretical efforts will not only bring us new insights into such novel materials but also pave the way to the new generation of molecule-based magnets.

Acknowledgment. This work was supported in Japan by the Grand-in-Aid for Scientific Research on Priority Area and Next Generation Super Computing Project (Nanoscience Program) from the MEXT of Japan, and in the USA by NSF Grant CHE-0716718, the Institute for Functional Nanomaterials (NSF Grant 0701525), the U.S. Environmental Protection Agency (EPA Grant No. RD-83385601), and Office of Basic Energy Sciences, U.S. Department of Energy, under Contract No. DE-AC05-00OR22725 with UT-Battelle, LLC. We thank the referees for their instructive suggestions, which made important contributions for the improvement of this work.

Supporting Information Available: Relative energies for other isomers of oxides of **2** (Figure S1), relative energies for **2a**−**d** calculated with different basis sets (Table S1), the $\langle S^2 \rangle$ values for NG oxides (Table S2), the energies and $\langle S^2 \rangle$ for **1d** at high-spin and low-spin states (Table S3), the full citation of ref 57, and the Cartesian coordinates for NG oxides. This material is available free of charge via the Internet at http://pubs.acs.org.

JA902878W